

Thermal Based Analysis of Continuous W-shaped rib in Solar Air Heater

M.Tech. Scholar Nitisha Sharma, M.Tech. Scholar Nilesh Singh, Prof. D.S. Rawat

Department of Mechanical Engineering,
JEC, Jabalpur,MP,India

Abstract-Augmentation of convective heat transfer of a rectangular duct with the help of baffles/ribs has been a common practice in the past few years. This concept is widely applied in enhancing the thermo-hydrodynamic efficiency of various industrial applications such as thermal power plants, heat exchangers, air conditioning components, refrigerators, chemical processing plants, automobile radiators and solar air heaters. Solar air heater is a device used to augment the temperature of air with the help of heat extracted from solar energy. These are cheap, have simple design, require less maintenance and are eco-friendly. As a result, they have major applications in seasoning of timber, drying of agricultural products, space heating, curing of clay/concrete building components and curing of industrial products. In this study CFD analysis for enhancement of heat transfer rate in solar air heater using w-shaped roughness has been done.

Keywords- Augmentation, convective heat transfer, rectangular duct

I. INTRODUCTION

Fossil fuel sources are confined and so the present scenario of energy consumption and growth are not sustainable in the longer term [1]. The energy demand for different applications can be attained by pick up of the solar energy efficiently. Solar energy is the most promising source of energy and the simplest and efficient way of using solar energy is to convert it into thermal energy for heating applications such as space heating, drying of agricultural products and various industrial applications by using solar air heater. The solar air heater is not efficient due to low convective heat transfer coefficient between absorber plate and flowing air.

The low rate of heat transfer coefficient is due to presence of a viscous sub-layer. Artificial roughness on the underside of the absorber plate breaks up the laminar sub-layer and increases heat transfer. Increased heat transfer makes the system more effective. Various investigators have investigated the effect of heat transfer and friction factor in various geometries of artificial roughness in a solar air heater duct. Solar air heaters are simple in design and construction. They are widely used as collection devices having applications such as space heating and crop drying. Efficiency of flat plate solar air heater is low because of low convective heat transfer coefficient between absorber plate and flowing air that increases absorber plate temperature, leading to higher heat losses to environment.

Low value of heat transfer coefficient is due to presence of laminar sub-layer that can be broken by providing artificial roughness on heat transferring surface [1]. Efforts for enhancing heat transfer have been directed toward artificially destroying or disturbing this laminar

sub-layer. Artificial roughness in form of ribs and in various configurations has been used to create turbulence near wall or to break laminar sub-layer. Artificial roughness results in high frictional losses leading to more power requirement for fluid flow. Hence turbulence has to be created in region very close to heat-transferring surface for breaking viscous sub-layer. Core fluid flow should not be unduly disturbed to limit increase in pumping requirement. This is done by keeping height of roughness elements small in comparison to duct dimensions [2].

Solar energy is one of the most useful renewable energy resources without any adverse effects on the environment. Solar energy is widely used for generating electricity, heating and various industrial applications. Solar air heaters (SAHs) are simple in design and generally used as solar thermal collectors [1]. SAHs are inexpensive and the most widely used collection devices because of their inherent simplicity. SAHs form the foremost component of a solar energy utilization system [2]. Figure 1 shows various components of a solar air heater. These air heaters absorb the irradiance and exchange it into thermal energy at the absorbing surface and then transfer this energy to a fluid flowing through the collector. An absorber plate is usually a thin metal sheet coated with an absorbing substance such as black or selective coating to absorb solar radiations. The glazing provides a rigid, protective structure for the entire collector assembly. Insulation beneath the absorber and fluid flow passages inhibits downward heat loss. SAHs are found in several solar energy applications, especially for space heating, timber seasoning and agriculture drying [3].

Conventional SAH has poor thermal performance due to low convective heat transfer rate from the heated plate to the air. The use of rib roughness on the heated plate is one

of the heat transfer augmentation methods employed in SAH systems. The idea of artificial roughness was initially applied to compact heat exchangers and cooling of gas turbine blades and electronic equipment [4]. Motivated by the improvements in thermal performance through the application of rib roughness in various configurations for gas turbine blade cooling, many researchers tried different roughness geometries to study their effect on the heat transfer of solar collectors and reported improvement in thermal performance [4–14]. Several experimental studies in SAH performance had been conducted to optimize the roughness elements of shape, size, orientation relative to flow direction [5].

This study presents CFD analysis on the thermal hydraulic characteristics of a three-dimensional SAH channel with square-sectioned discrete multi-V-pattern rib roughness. Average Nusselt number, friction factor and thermal hydraulic performance parameter were reported as functions of Reynolds numbers.

II. RESEARCH METHODOLOGY

1. Problem Formulation

The present work is concerned with carrying out three-dimensional simulations on an artificially roughened solar air heater, through which air flows. The air heater internal surface was roughened with the help of W-shape continuous ribs. Literature survey reveals that inclined and W-ribs give significant enhancement in heat transfer as compared to smooth plate. Secondary flow generated in above two cases has been cited as the main reason. In case of V-ribs four secondary vortices are generated. If the number of vortices is increased then theoretically it should increase heat transfer. But effect on friction needs to be investigated experimentally to evaluate its feasibility. Hence the present investigation has been taken up with objective of experimentation on W-shaped ribs as artificial roughness attached to underside of one broad wall of duct, to collect data on heat transfer and fluid flow characteristics. Data is presented in form of Nusselt number and friction factor plots as a function of geometrical parameters of artificial roughness and thermo-hydraulic performance plots to bring out clearly effect of these parameters and enhancement in heat transfer achieved as result of providing artificial roughness.

2. Computational domain

A rectangular section was considered. The domain on which numerical simulations were performed was three-dimensional. Their rectangular duct was of length 1500 mm, width 200 mm and thickness 25 mm. Fig. 2.1 shows the geometry of the computational domain. The rib roughness can be defined by the continuous rib with angle of attack is 90°. Simulation using CFD has been done by varying Re number from 2300 to 18000. Constant heat flux of value approximately 1000 W/m² was supplied

only on the upper wall of the absorber plate. Simulations were performed assuming the flow to be steady.

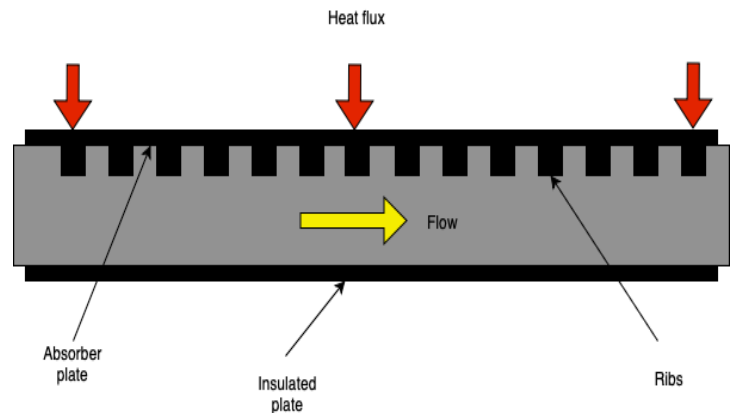


Fig. 1 Schematic of computational domain

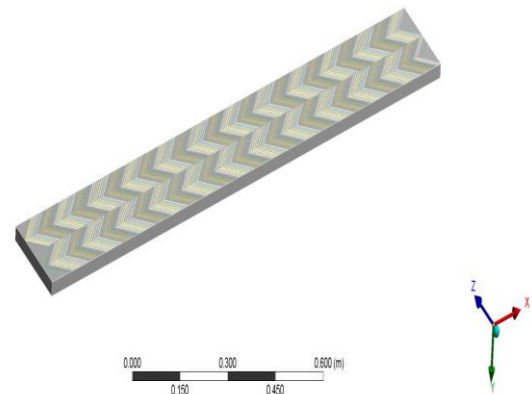


Fig. 2 Computational domain for CFD.

Table.1 Operating and Geometrical parameters used for CFD analysis

Operating and Geometrical parameters	Value / Range
Length of duct	1500 mm
Width of duct	200 mm
Thickness of duct	25 mm
Constant heat flux	1000 W/m ²
Range of Reynolds number	2300-18000
Height of rib	0.8 mm
Attack angle	60°

3. Governing differential equations

Continuity equation

$$\frac{\partial}{\partial x_i} (\rho u_i) = 0 \quad (2.1)$$

Momentum Equation

$$\frac{\partial}{\partial x_i}(\rho u_i u_j) = -\frac{\partial P}{\partial x_i} + \frac{\partial}{\partial x_j} \left[\mu \left(\frac{\partial u_i}{\partial x_j} + \frac{\partial u_j}{\partial x_i} \right) \right] + \frac{\partial}{\partial x_j} (-\rho u_i' u_j')$$

(2.2)

Energy equation

$$\frac{\partial}{\partial x_i}(\rho u_i T) = \frac{\partial}{\partial x_j} \left[(\Gamma + \Gamma_r) \frac{\partial T}{\partial x_j} \right]$$

(2.3)

4. Boundary Condition

On all the walls (including the roughened one) of the rectangular duct, no-slip boundary conditions were assigned. Constant heat flux of 1000 W/m² was decided to be the boundary condition at the upper wall of the absorber plate. At the inlet, uniform velocity with an inlet temperature of 300 K and at the exit, invariable pressure (atmospheric pressure) boundary conditions were assigned. All the other edges were assigned as walls with insulated boundary conditions, as shown in Fig. 2.3. The upper and other two side walls were assumed to be adiabatic.

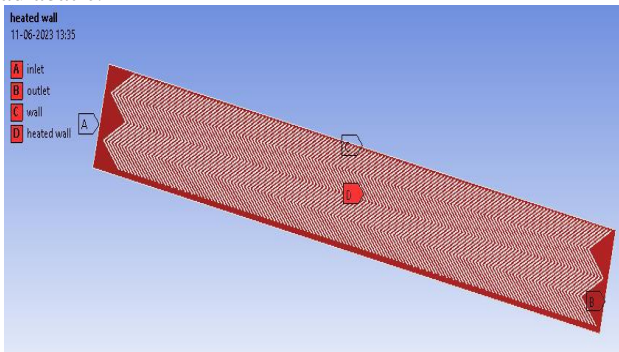


Fig. 2 Boundary condition for CFD analysis

5. Set up and flow specification

The generated mesh was then exported to FLUENT where the different flow and physical properties were specified. The appropriate turbulent model was selected and the energy option was switched on. The working fluid was air and aluminum, because of its higher absorptivity, was the absorber plate. Their thermo-physical properties are mentioned in Table 2

Table 2. Thermo-physical properties of aluminum as the absorber plate and air as the working fluid

Properties	Working fluid (air)	Absorber plate (aluminum)
Density, kg/m ³	1.1767	2719
Viscosity, kg/m-s	1.8582e-05	-
Specific heat (constant pressure), J/kg-K	1006.6	871
Prandtl number	0.714	-
Thermal conductivity, W/m-K	0.0262	202.4

Simulations were carried out under the following assumptions

- The absorber and duct wall were assumed to be isotropic and homogenous.
- Steady, turbulent and fully developed two-dimensional-flow.
- The absorber plate and the duct wall thermal conductivity were temperature-independent.
- Negligible heat losses and no radiation heat transfer.
- At the junction of wall and fluid, no-slip boundary conditions were assumed.
- The absorber plate and working fluid (air) properties were invariable at an average bulk temperature of 300 K.

Table 3 Estimation of velocity at different Reynolds number

Reynolds number	Velocity, m/s
2300	0.7558
4000	1.3144
8000	2.6287
10000	3.2859
15000	4.9289
18000	5.9147

6. Reduction of Data

Following equations have been used for the evaluation of relevant parameters:

$$q = mX C_p X (t_o - t_i) \quad (2.4)$$

$$h = q / [A_c X (t_p - t_f)] \quad (2.5)$$

$$Nu = (hX D_h) / k \quad (2.6)$$

Where Dh is hydraulic diameter

$$D_h = \frac{2ab}{a+b} \quad (2.7)$$

a is the height of the duct and b is the width of the duct

$$f = D_h X \Delta P / (2 XLX V^2 X \rho) \quad (2.8)$$

7. Best turbulent model selection

In order to determine which turbulent model would most accurately yield numerical results, the following methodology was adopted. CFD calculations were performed on a smooth duct (without ribs) and the friction factor and Nusselt number variation with “Re” results were extracted from the simulation. Heat flux was applied only on the top wall of the test duct, whereas the other side remained insulated. The turbulent model, namely RNG-k-epsilon, was chosen and their corresponding results in terms of Nusselt number alteration with Reynolds number were compared.

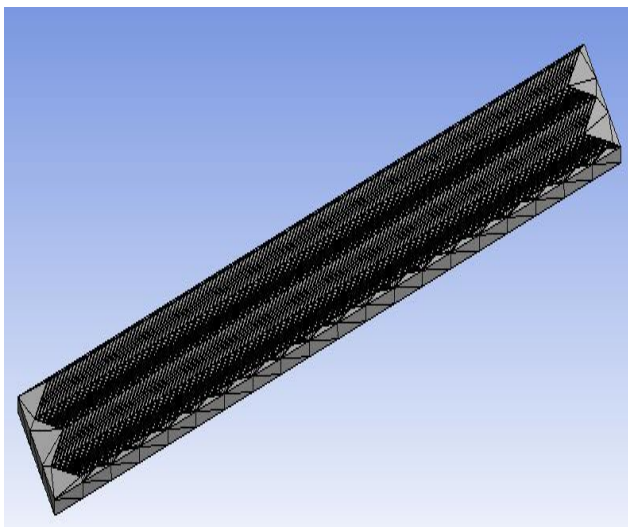
III. RESULTS AND DISCUSSION

1. Grid Independence Test

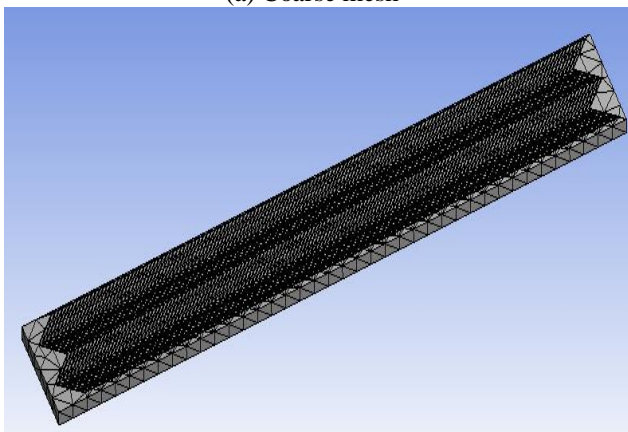
The grid independence test is a process used to find the optimal grid condition that has the smallest number of

grids without generating a difference in the numerical results based on the evaluation of various grid conditions. The grid generations were generated by using ANSYS DesignModeler and ANSYS Meshing. In this work, the fluid computational domain was only created because the adiabatic wall was assumed at domain boundary. Hence, the domain of the duct was ignored. The quadrilateral grids were generated inside the calculation domains with the help of the domain decomposition technique (Bumrunthaichai and Wattananusorn, 2019; Namkanisorn et al., 2022) to reduce the truncation errors (Bumrunthaichai, 2016).

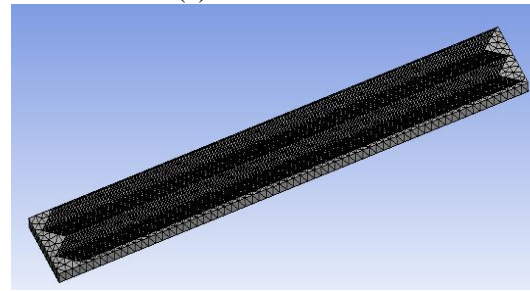
Further, the wall-refined grid generation as reported by Ruangtrakoon and Bumrunthaichai (2018) was adopted to control the near-wall grid sizes. The y^+ values of these near-wall grids were in the range of unity. The dimensionless wall distance, y^+ turbulent flow CFD simulation. It can be defined as $y^+ = \rho y_p u_{\tau}^2 / \mu$, where ρ is a fluid density, μ is a fluid viscosity, y_p is a normal distance from the wall to the near-wall computing node, and u_{τ} is the friction velocity. See also Bumrunthaichai (2022) for more information on y^+ . Here, the grid generations designs are shown in Fig. 3.



(a) Coarse mesh



(b) Medium mesh



(c) Fine mesh

Fig. 3 Grid independence test.

A comprehensive grid independence study was performed to ensure the grid independence of the results. There were two objectives of the grid independence test. First, the converged solution was obtained based on the boundary conditions and the physics involved, and not because of the mesh used. Second, the number of cells employed in the computational domain was optimized. The value of interest was the Nusselt number, and the optimum number of cells for the domain was >14 million.

2. Model Validation

Figs. 3.2 show comparison of simulation values and those predicted by correlations for Nusselt number of smooth duct proposed by modified Dittus-Boelter correlation for Nusselt number. Absolute percentage deviation between predicted and experimental results has been found to be within 5% for Nusselt number. Excellent agreement between simulation and predicted values establishes accuracy of measurement on CFD domain.

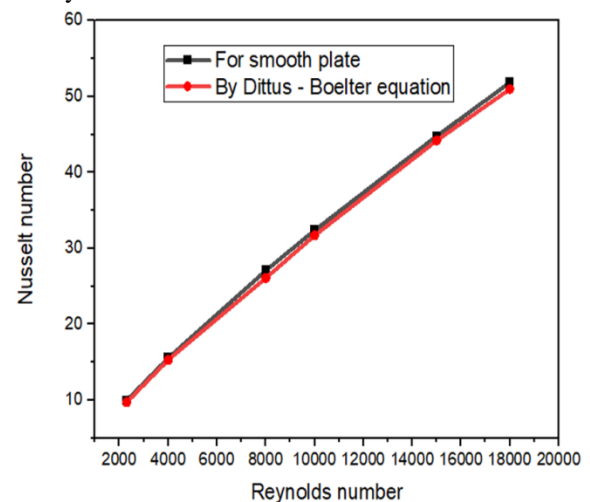


Fig. 4 Nusselt number validation.

Figs. 3.3 show comparison of simulation values and those predicted by correlations for friction factor of smooth duct proposed by modified Blasius correlation for friction factor. Absolute percentage deviation between predicted and experimental results has been found to be less than 5% for friction factor. Excellent agreement

between simulation and predicted values establishes accuracy of measurement on CFD domain.

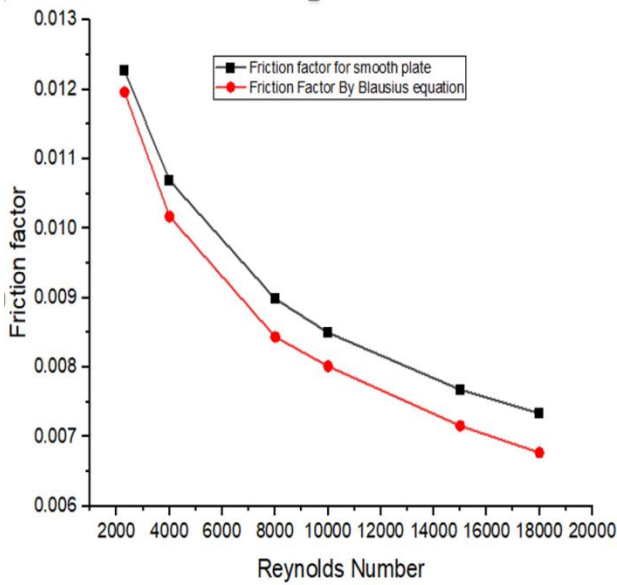
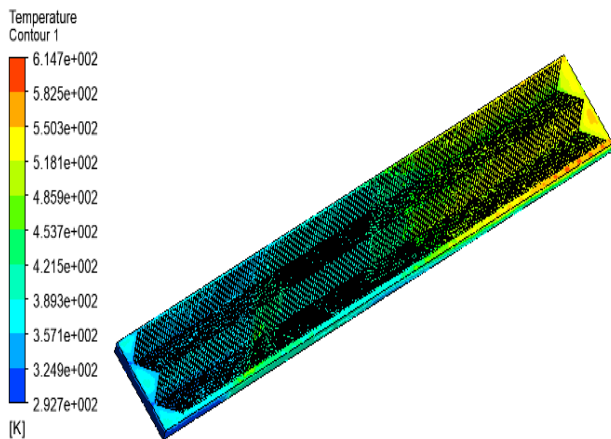
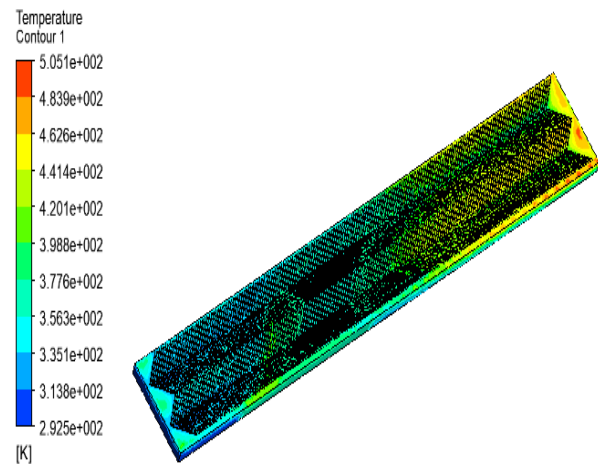


Fig. 4 Nusselt number validation

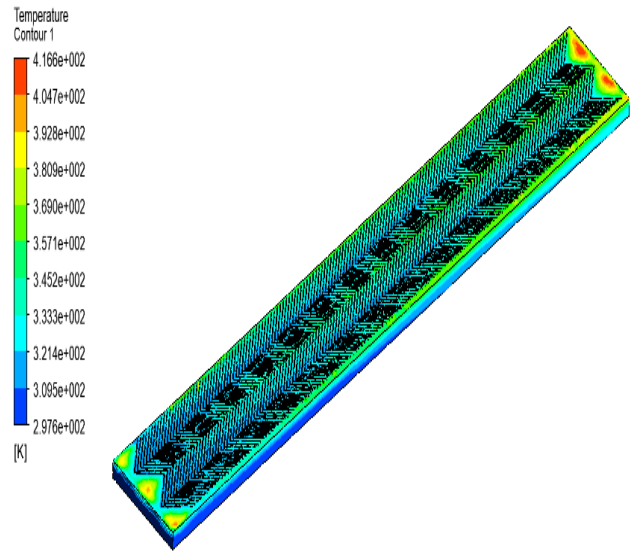
3. Temperature Profile



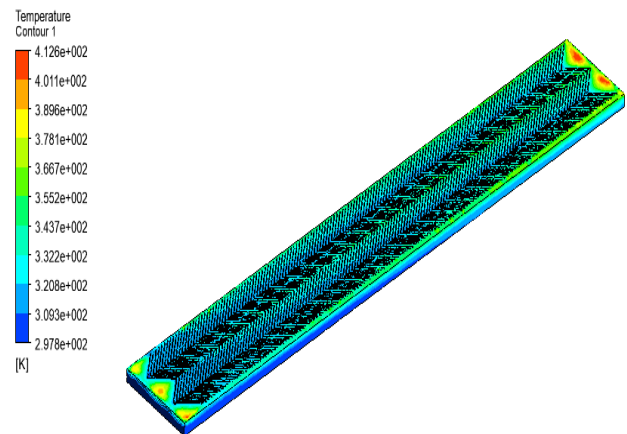
(a) Re= 2300



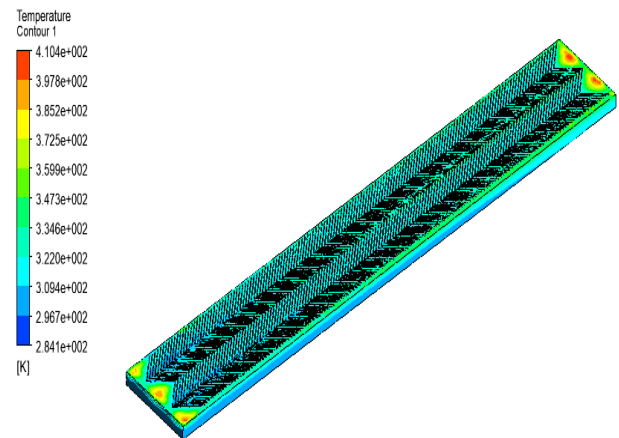
(b) Re= 4000



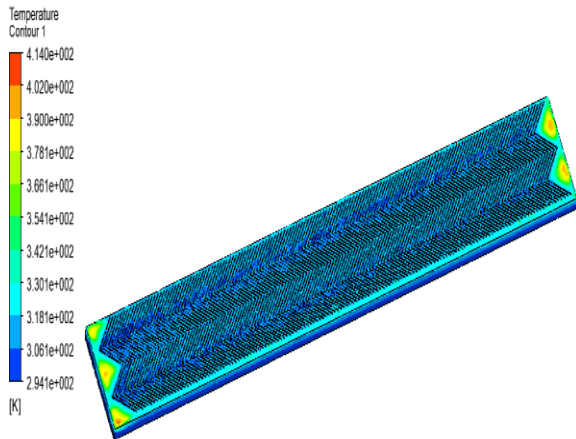
(c) Re= 8000



(d) Re= 10000



(e) Re=15000



(f) Re=18000

Fig.4 Temperature plot at different Reynolds number

Temperature vector contour plots at a different Reynolds number when pitch to height ratio is 10 are depicted in Fig. 3.4. The intensity of temperature can be seen in different colour (blue to red) at different location. There is an extreme regularity in the contours of instantaneous velocity due to the effect of ribs. Eddy formation is clearly shown in the contours plot, in the vicinity of ribs. The fluid flow experiences sudden expansion leading to a separation region at the rib downstream. This separation is followed by reattachment of the fluid ahead the next rib. The periodic circulation of reattachment of flow leads to the formation of a small secondary vortex near the absorber plate and fluid junction. The secondary vortices are much more strongly created in case of thin ribs. Furthermore, it is observed that the velocity of the fluid is accelerated lengthwise as it passes through the test channel. Hence greater amount of disturbances are observed in the laminar sub layer thereby leading to a reduction in conductive transfer of heat and a significant augmentation in convective transfer of heat.

7. Effect of Pitch to Rib- Height Ratio on Nusselt Number

Effect of relative roughness height on Nusselt number is shown in Fig3.5. The horizontal x-axis represents pitch-to-height ratio and y-axis represents Nusselt number. It is seen that increase in relative roughness height results in increase in heat transfer coefficient and friction factor. Further it is seen that rate of increase of Nusselt number is lower than that of friction factor. This may be due to the fact that at higher values of relative roughness height, reattachment of free shear layer might not occur and rate of heat transfer enhancement is not proportional to that of friction factor.

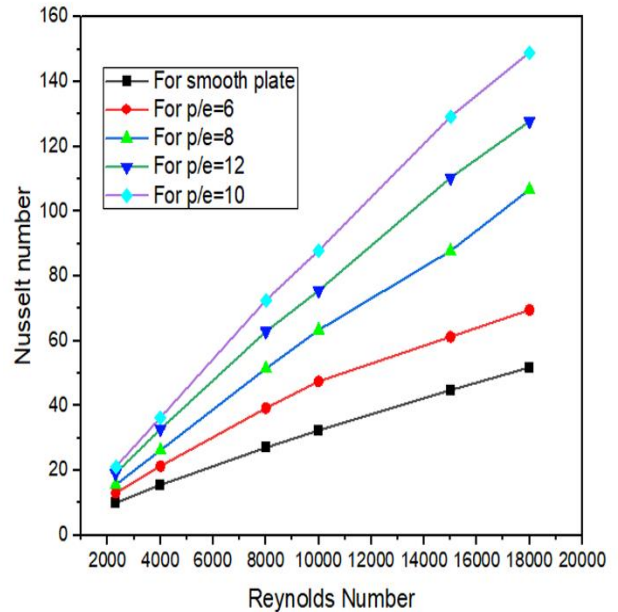


Fig.5 Variation of Nusselt at different pitch to rib- height ratio

8. Effect of Pitch to Rib- Height Ratio on Friction Factor

Effect of relative roughness height on friction factor is shown in Fig.3.6. The horizontal x-axis represents pitch-to-height ratio and y-axis represents friction factor. It is seen that increase in relative roughness height results in increase in heat transfer coefficient and friction factor. Further it is seen that rate of increase of Nusselt number is lower than that of friction factor. This may be due to the fact that at higher values of relative roughness height, reattachment of free shear layer might not occur and rate of heat transfer enhancement is not proportional to that of friction factor.

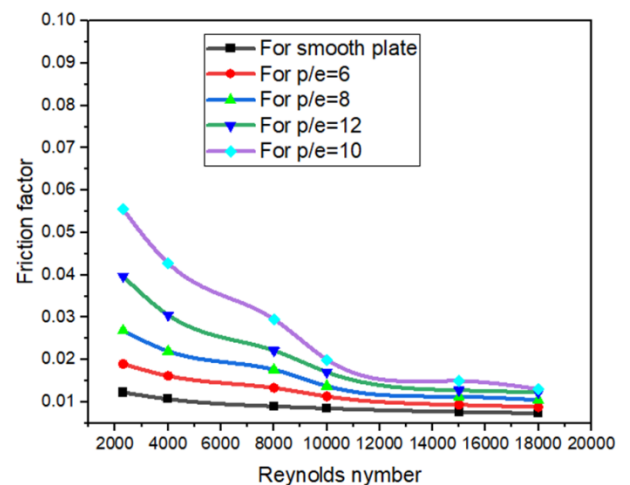


Fig.6: Variation of friction factor at different pitch to rib- height ratio

9. Assessment of Thermo-Hydraulic Performance

Artificial roughness on absorber plate results in enhancement of heat transfer. Enhancement is accompanied by increase in friction factor. Hence roughness geometry has to be so selected such that heat transfer is maximized while friction losses are at minimum value. This is fulfilled by considering heat transfer and friction characteristics simultaneously. Parameter that facilitates simultaneous consideration of thermal and hydraulic performance is given by Webb and Eckert [40] as

$$\eta = \left(\frac{Nur}{Nus}\right) / \left(\frac{fr}{fs}\right)$$

It is evident that only a heated wall roughness that yields a performance parameter value greater than unity is useful. The higher the value of this parameter, the better the solar air channel performance.

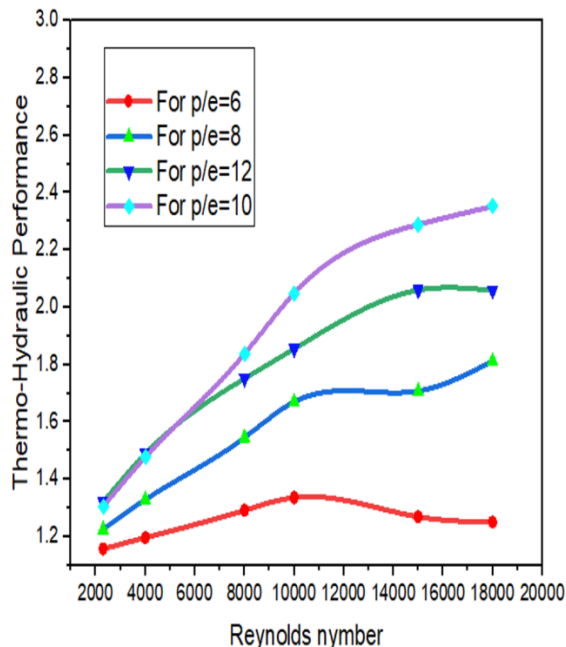


Fig.7 Variation of thermo-hydraulic performance at different pitch to rib- height ratio

The plot of thermo-hydraulic performance parameter as a function of Re at different values of p/e is shown in Figure 3.7. The horizontal x-axis represents the horizontal x-axis represents pitch-to-height ratio and y-axis represents thermo-hydraulic performance. It is seen that thermo-hydraulic performance increases with an increase in the p/e . This basic reason of creating a discrete rib is that, the discrete flow promotes local turbulence and flow mixing along the discrete flow region while the rib induced secondary flow is maintained in the duct. At the same time too small a discrete width will also not allow sufficient amount of secondary flow fluid to pass through and hence the turbulence level will remain low.

IV. CONCLUSION

Nusselt number increases whereas friction factor decreases with increase of Reynolds number. Values of friction factor and Nusselt number are higher as compared to those for smooth absorber plate. This is due to change in flow characteristics because of roughness that causes flow separation, reattachments and generation of secondary flow.

Rate of increase of Nusselt number with increasing Reynolds number is lower than rate of increase of friction factor because at higher values of relative roughness height, reattachment of free shear layer does not occur and rate of heat transfer enhancement is not proportional to that of friction factor and it is maximum at $p/e=10$.

Flow separation and secondary flow resulting from presence of W-shaped ribs and movement of vortices combine to give optimum value of angle of attack. Thermo-hydraulic performance is improved with different pitch to rib- height ratio and it is maximum at $p/e=10$.

Comparison of simulation values of Nusselt number and those predicted by correlation lie within deviation range of 5% whereas in case of friction factor, within 5%. It can therefore be concluded that correlations for prediction of Nusselt number and friction factor are reasonably satisfactory. For all the cases considered in this study, increase in Reynolds number leads to augmentation in Nusselt number. When ribs/baffles are introduced just beneath the collector plate, there was a considerable alteration in the heat transfer coefficient of air.

REFERENCES

1. Agrawal, Y., Yugbodh, K., Ahmed, S. F., Jain, E., Bhagoria, J. L., Gautam, A., & Mishra, A. (2023). Experimental investigation of heat transfer and flow analysis of artificially roughened solar air heater by using double arc reverse shaped roughness with gap on the absorber plate. *Materials Today: Proceedings*, 78, 403-413.
2. Fadala, G. M., & Yousef, A. H. (2023). The effect of artificial roughness on performance of solar air heater (SAH): A review study. In *AIP Conference Proceedings* (Vol. 2776, No. 1, p. 050008). AIP Publishing LLC.
3. Chaurasia, S., Goel, V., & Debbarma, A. (2023). Impact of hybrid roughness geometry on heat transfer augmentation in solar air heater: A review. *Solar Energy*.
4. Saxena, R., Pachorkar, P., Jain, A., Majumder, H., Pandey, K. K., Mishra, S. K., & Kalbande, V. P. (2023). Performance enhancement of solar air heater using artificial roughness. *Materials Today: Proceedings*.
5. Yadav, A. K., Choudhary, M., & Singh, A. P. (2023). Assessment of solar air heater performance using a

- variety of artificially roughened components. *Materials Today: Proceedings*.
6. Singh, V. P., Jain, S., & Gupta, J. M. L. (2023). Analysis of the effect of perforation in multi-v rib artificial roughened single pass solar air heater:-Part A. *Experimental Heat Transfer*, 36(2), 163-182.
 7. Kumar, D., & Layek, A. (2023). Heat Transfer Enhancement of Solar Air Heater Having Twisted V-Shaped Staggered Roughness Over Absorber Plate. *Arabian Journal for Science and Engineering*, 48(3), 3931-3946.
 8. Arya, N., Goel, V., & Sunden, B. (2023). Solar air heater performance enhancement with differently shaped miniature combined with dimple shaped roughness: CFD and experimental analysis. *Solar Energy*, 250, 33-50.
 9. Kumar, D., & Layek, A. (2022). Parametric analysis of artificial rib roughness for the enhancement of thermohydraulic performance of solar air heater: A review. *Materials Today: Proceedings*, 57, 1127-1135.
 10. Singh, H., Singh, H., & Kishore, C. (2022). CFD numerical investigation of Heat transfer characteristics of Y-shaped solar air heater. *Materials Today: Proceedings*, 52, 2003-2013.
 11. Yadav, A. S., Gupta, S., Agrawal, A., Saxena, R., Agrawal, N., & Nashine, S. (2022). Performance enhancement of solar air heater by attaching artificial rib roughness on the absorber Plate. *Materials Today: Proceedings*, 63, 706-717.
 12. Bhuvad, S. S., Azad, R., & Lanjewar, A. (2022). Thermal performance analysis of apex-up discrete arc ribs solar air heater-an experimental study. *Renewable Energy*, 185, 403-415.